

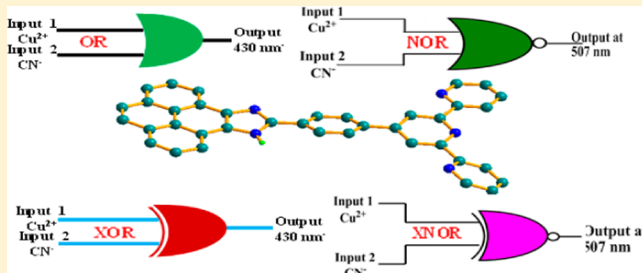
Demonstration of Multiple Logic Operations in a Heteroditopic Pyrene–Phenylimidazole–Terpyridine Conjugate Based on Optical Responses by Selective Anions and Cations: An Experimental and Theoretical Investigation

Srikanta Karmakar, Dinesh Maity, Sourav Mardanya, and Sujoy Baitalik*

Department of Chemistry, Inorganic Chemistry Section, Jadavpur University, Kolkata 700 032, India

 *Supporting Information*

ABSTRACT: Combined experimental and density functional theory (DFT) and time-dependent density functional theory (TD-DFT) studies were carried out to investigate the structural and electronic properties of a terpyridyl-phenylimidazole system covalently linked to pyrene, 10-(4-[2,2':6',2"-terpyridine]terpyridin-4'-yl-phenyl)-9H-9,11-diazacyclopenta[e]pyrene (tpy-HImzPy). X-ray crystal structure determination shows that the compound crystallized in monoclinic form with the space group $P2_1/c$. The anion and cation sensing properties of tpy-HImzPy were thoroughly studied in dimethyl sulfoxide and in mixed dimethyl sulfoxide–water medium through different channels such as absorption, steady-state and time-resolved emission, and ^1H NMR spectroscopic methods. In this work, by grafting the pyrene moiety into the terpyridyl chelating unit, an intraligand-charge-transfer sensitive chromophore has been developed whose absorption and emission behaviors are highly sensitive to selective anions and cations, and the response profiles in terms of absorption or emission intensity and wavelength toward the tested ions varied quite a lot. On the basis of these observations, we developed a unique molecular system capable of performing multiple logic functions such as INHIBIT, OR, XOR, NOR, and XNOR by simply varying the combination and level of various ionic inputs in a systematic manner. In this work, we will also be particularly interested to see the effect of selective anion and cation on the optical properties of receptor by means of computational studies and correlate them with the experimentally observed data.



1. INTRODUCTION

Since the first realization of information processing and computation at the molecular level by de Silva in 1993, lots of efforts have been devoted to the development of the electronic devices on a nanometer scale by using single molecules based on their spectral responses toward the external stimuli.^{1–5} In computers, information processing is based on the principles of Boolean algebra; a system for mathematical analysis through logic operation(s).^{6,7} Logic gates are the devices used to perform binary arithmetic and logical operations which constitutes the basis of modern computers.^{1–5,8–15} The computation at the molecular level is thus possible only with the molecular logic gate, which are capable of integrating simple logic gates into combinational circuits.^{1–7} It may be mentioned that Boolean binary logic is based on precise objective knowledge; that is, the statements are true or false, reducible to strings of zeros and ones only. But in reality it is not always possible to store accurate information while describing a complex molecular system and very often the acquired data and knowledge suffer from some sort of uncertainty. In these cases, an alternative computing strategy based on Fuzzy logic can be adopted.^{16–21} Fuzzy logic is thus an extension of Boolean logic [defined by the binary pairs (0, 1) or (False, True)] which includes the whole continuous interval

[0, 1]. Presently, the Fuzzy logic system is drawing increasing attention because of its probable potential for developing Artificial Intelligence.^{16–21}

Several molecular systems performing Boolean and Fuzzy logic operations and responding to a large variety of activating input signals (e.g., light, electrical, magnetic, and chemical) were developed in the past two decades.^{8–41} In general, the reported systems were based on the modulation of their emission properties by different combinations of external inputs. However, relatively few molecular systems are available that can mimic multiple logic functions by treating multiple inputs and utilizing both absorption and emission responses.^{18,34–40} Thus, there remains scope for designing and synthesizing molecules that can perform multiple logic functions. It appears that smart functional molecules with distinct anion and cation coordination site(s) could be potential candidates for performing multiple logic operations because the absorption and emission properties of the ditopic ligands can be modulated to a significant extent by appropriate combination of anion and cation. During the past

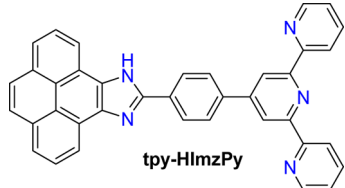
Received: June 4, 2014

Revised: September 12, 2014

Published: September 12, 2014

few years we are interested in designing polypyridyl-imidazole based sensors for recognizing both anion and cation in solution through different channels.^{42–46} In this report, we have utilized a terpyridyl-phenylimidazole system covalently linked to pyrene, 10-(4-[2,2':6',2"-terpyridine]terpyridin-4'-yl-phenyl)-9H-9,11-diaza-cyclopenta[e]pyrene (tpy-HImzPy, Chart 1) for the

Chart 1



construction of multifunctional and multiply configurable logic gate system.⁴⁶ In addition to the terpyridine coordinating site for metals, the novel ligand also possesses an imidazole NH proton that can be utilized for recognition of selective anions either through hydrogen bonding interaction or by proton-transfer reaction. In the design of a ligand, a pyrene core has been introduced because of its rigid geometry and interesting photophysical properties. It is well-known that pyrene and its derivatives have been extensively used in a variety of applications such as organic light emitting diodes, ion sensors, and biological imaging. Moreover, by grafting the pyrene moiety into the terpyridyl chelating unit, an ICT-sensitive chromophore has been developed whose absorption and emission behaviors are highly sensitive to selective anions and cations, and the response profiles in terms of absorption or emission intensity and wavelength toward the tested ions varied quite a lot. On the basis of these observations, we developed a unique molecular system capable of performing multiple Boolean logic functions such as INHIBIT, OR, XOR, NOR and XNOR by using various ionic inputs in a sequential patterns. In addition, we have also implemented Fuzzy logic operations on this system by exploiting the luminescence characteristics of tpy-HImzPy by simply varying the combination and level of selected anions and cations in a systematic manner. In this report we will also carry out density functional theory (DFT) and time-dependent density functional theory (TD-DFT) calculations in both ground and excited state of the compound for better understanding of the electronic structures and spectroscopic properties. In particular, we will be interested to see the effect of selective anion and cation on the optical properties of receptor by means of computational studies and correlate them with the experimentally observed data.

2. EXPERIMENTAL SECTION

2.1. Materials. Reagent grade chemicals were obtained from Sigma-Aldrich and used without further purifications. Tpy-HImzPy was prepared from pyrene-4,5-dione and 4'-(*p*-formylphenyl)-2,2':6',2"-terpyridine (tpy-PhCHO) and was thoroughly characterized by using a previously reported procedure by us.⁴⁶

2.2. Physical Measurements. High-resolution electrospray mass spectra (ESI-MS) were acquired on a Waters Xevo G2 QTOF mass spectrometer. ¹H NMR spectra were recorded on a Bruker Avance DPX 500 spectrometer using DMSO-*d*₆ solutions. Electronic absorption spectra were recorded on a Shimadzu UV 1800 spectrophotometer. Steady-state photoluminescence

spectra were recorded on a Perkin-Elmer LS55 fluorescence spectrophotometer. The quantum yield of the receptor was determined by a relative method using quinine sulfate as the standard.⁴⁷ Luminescence lifetimes were recorded by a time-correlated single-photon-counting (TCSPC) technique at room temperature. For the TCSPC measurement, the photoexcitation was made at 370 nm using a nanosecond diode laser. The luminescence decay data were collected on a Hamamatsu MCP photomultiplier (R3809) and were analyzed by using IBH DAS6 software. The sensing studies of the receptor with different anions and cations were carried out in dimethyl sulfoxide as well as in dimethyl sulfoxide–water medium. TBA salts of different anions and hydrated perchlorate salts of the metals were used for titration experiments.

2.3. X-ray Crystal Structure Determination. Single crystals of tpy-HImzPy were obtained by diffusing methanol into its DMF solution. X-ray diffraction data for the crystal were collected on a Bruker-AXS SMART APEX II diffractometer at room temperature equipped with CCD detector using graphite-monochromated Mo K α radiation ($\lambda = 0.710\,73\text{ \AA}$). Crystallographic data are given in Table S1 (Supporting Information). The data were processed with SAINT⁴⁸ and absorption corrections were made with SADABS.⁴⁸ The structure was solved by direct and Fourier methods and refined by full-matrix least-squares based on F^2 using the WINGX software which utilizes SHELX-97.⁴⁹ For structure solution and refinement, the SHELXTL software package was used.⁵⁰ The non-hydrogen atoms were refined anisotropically, and the hydrogen atoms were placed with fixed thermal parameters at idealized positions. The final least-squares refinement ($I > 200\sigma(I)$) converged to reasonably good *R* values (Table S1, Supporting Information). CCDC reference number: 996148 for tpy-HImzPy.

2.4. Fuzzy Logic Analysis. Fuzzy analysis has been done with the help of Fuzzy Logic Toolbox in Matlab 7.1 and is implemented by Mamdani's method with the centroid defuzzification.^{51,52} A Fuzzy logic system (FLS) is composed of four primary elements: fuzzifier, fuzzy rule base, inference engine, and the defuzzifier. The crisp measured data (e.g., quantum yield of fluorescence) have been transformed into suitable linguistic (i.e., fuzzy sets, for example; fluorescence is low) values by means of the fuzzifier. The kernel of a FLS is an inference engine capable of simulating human decision making by performing approximate reasoning to achieve desired results. The fuzzifier maps the crisp inputs into fuzzy sets, which are subsequently used as inputs to the inference engine, whereas the defuzzifier maps the fuzzy sets produced by the inference engine into crisp numbers. Among several defuzzifier techniques (bisector, largest of the maximum and smallest of the maximum, middle of the maximum) we have employed the centroid method in this work. In the centroid defuzzification technique, the "center of mass" of the result provides the crisp value. The first step is to fuzzify the crisp inputs Φ_F (quantum yield) and then to determine the degree to which they belong to each of the appropriate fuzzy sets via membership functions (μ_{low} , μ_{medium} , μ_{high}). In the subsequent step, we apply a fuzzy implication operator to obtain a new fuzzy set. In the third step, the outputs obtained for each rule in the second step were combined into a single fuzzy set by means of fuzzy aggregation operator. Finally, via a centroid defuzzification method, the crisp values can be obtained.^{51,52}

2.5. Computational Methods. All calculations were performed with the Gaussian 09 program⁵³ package employing the DFT method with Becke's three-parameter hybrid functional

and Lee–Yang–Parr's gradient corrected correlation functional (B3LYP) level of theory using 6311-G basis set for the ligands (tpy-HImzPy and tpy-ImzPy). For the three metal complexes, the 6311-G basis set was used for C, H, and N atoms, whereas the LanL2DZ basis set was utilized for Fe, Cu, and Zn metals.^{54,55} Geometries were fully optimized using the criteria of the respective programs. To compute the UV–vis absorption transitions of the compounds, the singlet excited-state geometries corresponding to the vertical excitations were optimized using the time-dependent DFT (TD-DFT) scheme starting with the ground-state geometries optimized in solution phase.^{56–59} The excitation energies were simulated by PCM model for the ligand and the CPCM model for the metal complexes.^{60,61} The geometries of the lowest energy singlet excited states of tpy-HImzPy and tpy-ImzPy were also optimized in dimethyl sulfoxide by using the TD-DFT method and employing the PCM models to calculate the emission energies. Orbital and fractional contribution analysis were done with Gauss View⁶² and Gauss Sum 2.1.⁶³

3. RESULTS AND DISCUSSION

3.1. Characterization of Tpy-HImzPy by Single Crystal X-ray Crystallography. The ligand crystallized in monoclinic form with the space group $P2_1/c$. The Oak Ridge Thermal Ellipsoid Plot (ORTEP) along with atom label are depicted in Figure 1, whereas crystallographic data and the bond distances

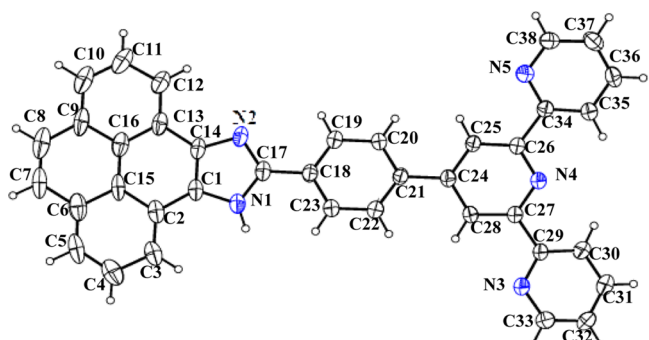


Figure 1. ORTEP representation of tpy-HImzPy showing 30% probability of thermal ellipsoid.

and angles are given in Tables S1–S3 (Supporting Information). Structural projections indicate the terpyridine moiety adopts a transoid arrangement about the interannular C–C bonds.⁴³ The dihedral angles between the central pyridine plane and the two lateral ones are 9.14 and 19.92°, and the dihedral angle between

the phenyl group attached to the central pyridine and imidazole moiety is 15.92°. It is interesting to note that the NH proton of the imidazole ring is involved in a strong intermolecular hydrogen bonding interaction with the O atom of solvated MeOH, forming an infinite chain with the N–H and O–H distance being 2.072 and 1.998 Å, respectively (Figure S1, Supporting Information).

3.2. Absorption and Emission Properties. Absorption and emission spectral behaviors of the receptor were studied in few selected solvents (Figure 2, and Figure S2, Supporting Information), and the relevant spectral data are given in Table 1. The higher energy band ranging between 279 and 303 nm seems to be due to $\pi-\pi^*$ transition whereas the lowest energy band lying between 349 and 394 nm is due to intraligand charge-transfer (ILCT) transition of the terpyridyl–imidazole ligand. Upon excitation, an intense emission band is observed that exhibits a solvatochromic shift of about 67 nm from nonpolar (ethyl acetate, 457 nm) to polar solvent (methanol, 524 nm), indicating an excited-state ILCT process (Figure 2a). Luminescence lifetimes of the receptor were also recorded in different solvents, and their decay profiles along with the lifetimes are shown in Figure 2b. It is evident that lifetime of the receptor increases in general with the polarity of the solvents. Moreover, a larger lifetime in polar solvents compared to that in less polar solvents also confirms the CT state of the emission processes (Figure 2b).^{64,65}

3.3. Spectral Responses of Tpy-HImzPy with Anions. The anion sensing properties of tpy-HImzPy were studied in dimethyl sulfoxide through different channels such as absorption, emission, and ^1H NMR spectroscopic methods. Upon the addition of 12 equiv of different anions, the absorption maxima at 356, 372, and 394 nm are red-shifted and merged to 428 nm with evolution of bright yellow color only in the presence of F^- and CN^- among all other studied anions (Figure 3a and Figure S3a, Supporting Information). Similar addition of the anions leads to the red shift of the emission maximum from 507 to 560 nm with concomitant quenching only with F^- and CN^- among all other studied anions (Figure 3b and Figure S3b, Supporting Information).

To get insight into the interaction between tpy-HImzPy and anions, UV–vis absorption and emission titrations were carried out with different anions (Figure 4 and Figure S3–S5 and Figure S7, Supporting Information). Figure 4a and Figure S3a (Supporting Information) show that upon incremental addition of both F^- and CN^- , the absorption maxima at 394 nm and in the range between 356 and 372 nm gradually decrease in intensity with a concomitant increase in intensity at 294 and 428 nm, respectively, with four well-defined isosbestic points in each case.

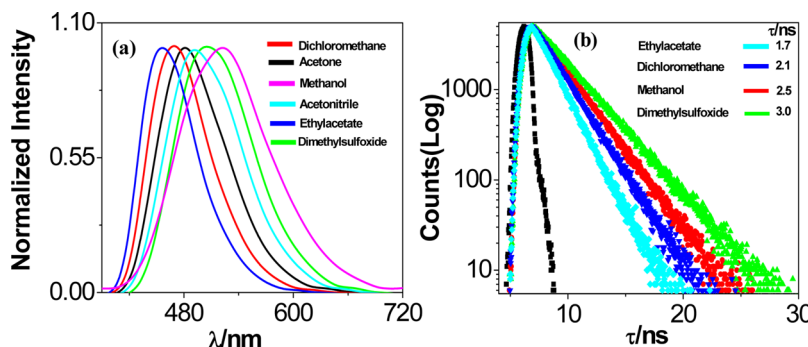


Figure 2. Steady-state luminescence (a) and excited-state fluorescence decay profiles (b) of tpy-HImzPy in different solvents.

Table 1. Photophysical Data of tpy-HImzPy in Different Solvents

solvents	absorption, λ_{\max}/nm ($\epsilon/\text{M}^{-1}\text{cm}^{-1}$)	emission	
		λ_{\max}/nm	Φ
chloroform	392 (32200), 370 (sh) (35300), 354 (45400), 303 (br) (53100), 292 (66150), 280 (sh) (57950)	466	0.28
dichloromethane	391 (15400), 368 (sh) (17300), 351 (br) (21800) 302 (sh) (24850), 291 (30900), 279 (sh) (26700)	470	0.31
ethanol	390 (23000), 368 (sh) (22000), 352 (31850), 288 (47200), 278 (sh) (40050)	498	0.16
methanol	387 (15150), 368 (sh) (14250), 349 (br) (21950), 288 (32850)	524	0.38
acetone	391 (32800), 369 (sh) (33300), 352 (br) (43450)	482	0.23
acetonitrile	390 (15100), 369 (sh) (14800), 350 (br) (19550), 301 (br) (21400), 290 (26950), 276 (sh) (22400)	493	0.26
dimethylformamide	392 (42350), 369 (sh) (43250), 355 (54350), 293 (73750), 281 (sh) (65050)	497	0.17
dimethyl sulfoxide	394 (32980), 372 (sh) (31400), 356 (38890), 294 (54890)	507	0.24
ethyl acetate	391 (26600), 368 (sh) (27500), 353 (34500), 301 (sh) (38700), 291 (46800), 278 (40150)	457	0.32

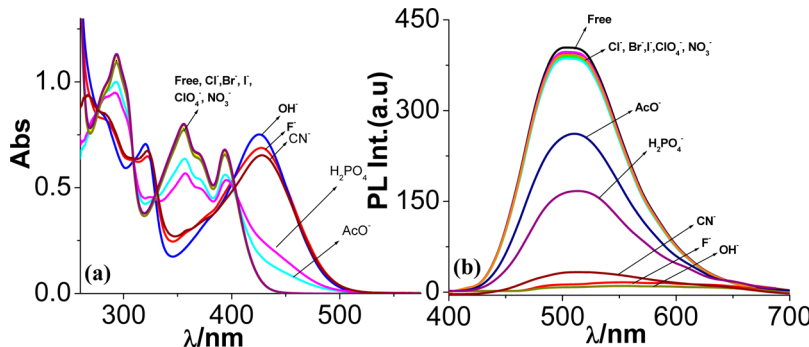
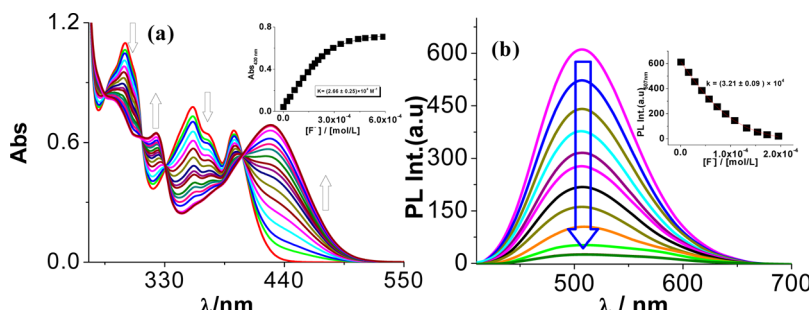
**Figure 3.** Change in UV-vis absorption (a) and luminescence (b) spectrum of tpy-HImzPy in dimethyl sulfoxide upon the addition of different anions as TBA salts.**Figure 4.** Change in UV-vis absorption (a) and luminescence (b) spectrum of tpy-HImzPy on incremental addition of F^- in dimethyl sulfoxide.

Figure 4b and Figure S3b (Supporting Information) show that upon incremental addition of F^- and CN^- , gradual quenching along with a red shift of emission at 507 nm occurs. The changes in the emission decay profiles of tpy-HImzPy upon incremental addition of F^- show that decays exhibited complex kinetics that can be fitted with a sum of two exponentials compared with monoexponential decay behavior of the free receptor (Figure S6, Supporting Information). Moreover, the lifetime of the second component gradually increases whereas the lifetime of the first component gradually decreases. Lifetime data indicate that the deprotonated receptor lives longer than its protonated counterpart. Absorption and emission titrations of the tpy-HImzPy were also carried out with tetrabutylammonium hydroxide (TBAOH). The spectral pattern obtained with OH^- (Figure S7, Supporting Information) has a close resemblance to the spectra of the receptor with F^- and, to a lesser extent, to CN^- . The result indicates that the imidazole NH proton is being deprotonated with an excess of the F^- and CN^- ions. The values of the equilibrium constants (K) defining quantitatively the interaction between tpy-HImzPy and the anions are listed in Table 2.

Table 2. Equilibrium/Binding Constants^a (K, M^{-1}) for tpy-HImzPy toward Various Anions and Cations in Dimethyl Sulfoxide at 298 K

Anions ($K \times 10^4$)	absorption	emission
F^-	2.66	3.21
CN^-	3.68	3.12
AcO^-	0.56	0.35
H_2PO_4^-	0.14	0.11
Cations ($K \times 10^7$)		
Fe^{2+}	4.85	7.21
Cu^{2+}	3.66	5.65
Zn^{2+}	4.22	3.12

^atert-Butyl salts of the respective anions and perchlorate salts of cations were used for the studies. Estimated errors were <15%.

The red shift of the spectral band can be attributed to anion-induced deprotonation of the imidazole NH proton of tpy-HImzPy, which increases the electron density at the imidazole fragment leading to lowering of the band energy. The excellent

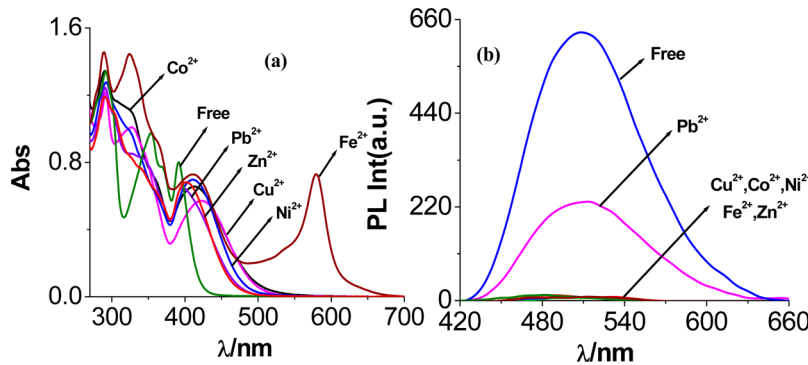


Figure 5. Change in UV–vis absorption (a) and luminescence (b) spectrum of tpy-HImzPy in dimethyl sulfoxide when treated with various metal cations as their perchlorate salts.

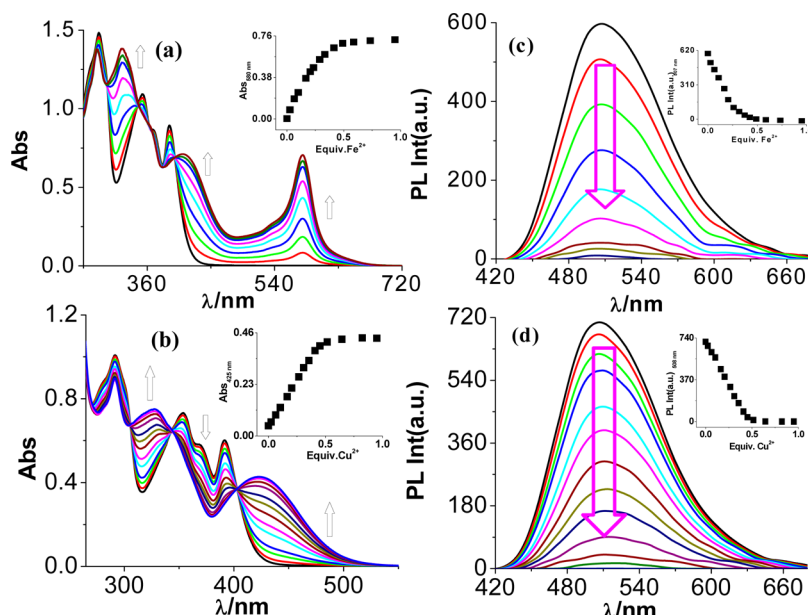


Figure 6. Change in UV–vis absorption (a and b, respectively) and luminescence (c and d, respectively) spectrum of tpy-HImzPy on incremental addition of Fe²⁺ and Cu²⁺, respectively, in dimethyl sulfoxide.

selectivity of tpy-HImzPy for F⁻ and CN⁻ is evident from the pronounced differences in absorption and emission spectral behavior and also from color changes. Based on the absorption and emission titrations, detection limits of tpy-HImzPy for F⁻ in dimethyl sulfoxide are 4.16×10^{-8} and 5.01×10^{-8} M, respectively (Figures S8 and S9, Supporting Information). When water-containing solvents such as dimethyl sulfoxide–water (9:1 v/v) are used, a similar type of sensing behavior is observed with the extent of shift lower compared with that for pure dimethyl sulfoxide (Figure S10, Supporting Information). In this case, a large excess of F⁻ is needed.

Figure S11 (Supporting Information) shows the ¹H NMR spectral change of tpy-HImzPy in the presence of 12 equiv of F⁻ in DMSO-*d*₆. Interestingly, the signal at 13.90 ppm due to the NH proton is completely removed by the F⁻ ion. Moreover, the resonances due to phenyl as well as the pyrenyl-imidazole moiety protons slightly upfield shifted, whereas the chemical shifts for the tpy protons remain almost constant. The small upfield shift of phenyl and pyrenyl-imidazole protons is due to increase of electron density at this site due to delocalization of the negative charge of the imidazole ring brought about by N–H deprotonation.

3.4. Spectral Responses of Tpy-HImzPy with Cations.

Figure 5 represents the changes in the absorption and emission spectral profiles upon addition of 0.5 equiv of different metal ions. Fe²⁺ exhibits a strong band at 585 nm with evolution of violet color in contrast to other metal ions. A huge spectral red shift from 394 to 585 nm in the case of Fe²⁺ over the other metal ions suggests that the receptor can act as an effective chemosensor toward the detection of Fe²⁺ in solution. Addition of the metals ions leads to emission quenching of the receptor at 507 nm in all cases. Parts a and b of Figure 6 show the spectral changes that take place upon incremental addition of Fe(ClO₄)₂ and Cu(ClO₄)₂ to the receptor, respectively. As may be noted, the new band evolved at 585 nm increases linearly with the incremental addition of Fe²⁺ until the [Fe²⁺]/[tpy-HImzPy] reaches 0.5. The titration profile and well-defined isosbestic points at 400, 347, and 303 nm indicate the single conversion of free tpy-HImzPy to [Fe(tpy-HImzPy)₂]²⁺. On the other hand, with the progressive addition of Cu(ClO₄)₂, diminution of the intensity of the major peak at 394 nm with a simultaneous increase of absorbance at 414 and 318 nm occurs. Parts c and d of Figure 6 show the quenching of emission intensity of the receptor on incremental addition of Fe(ClO₄)₂ and Cu(ClO₄)₂, respectively. Absorption and emission titrations with incremental

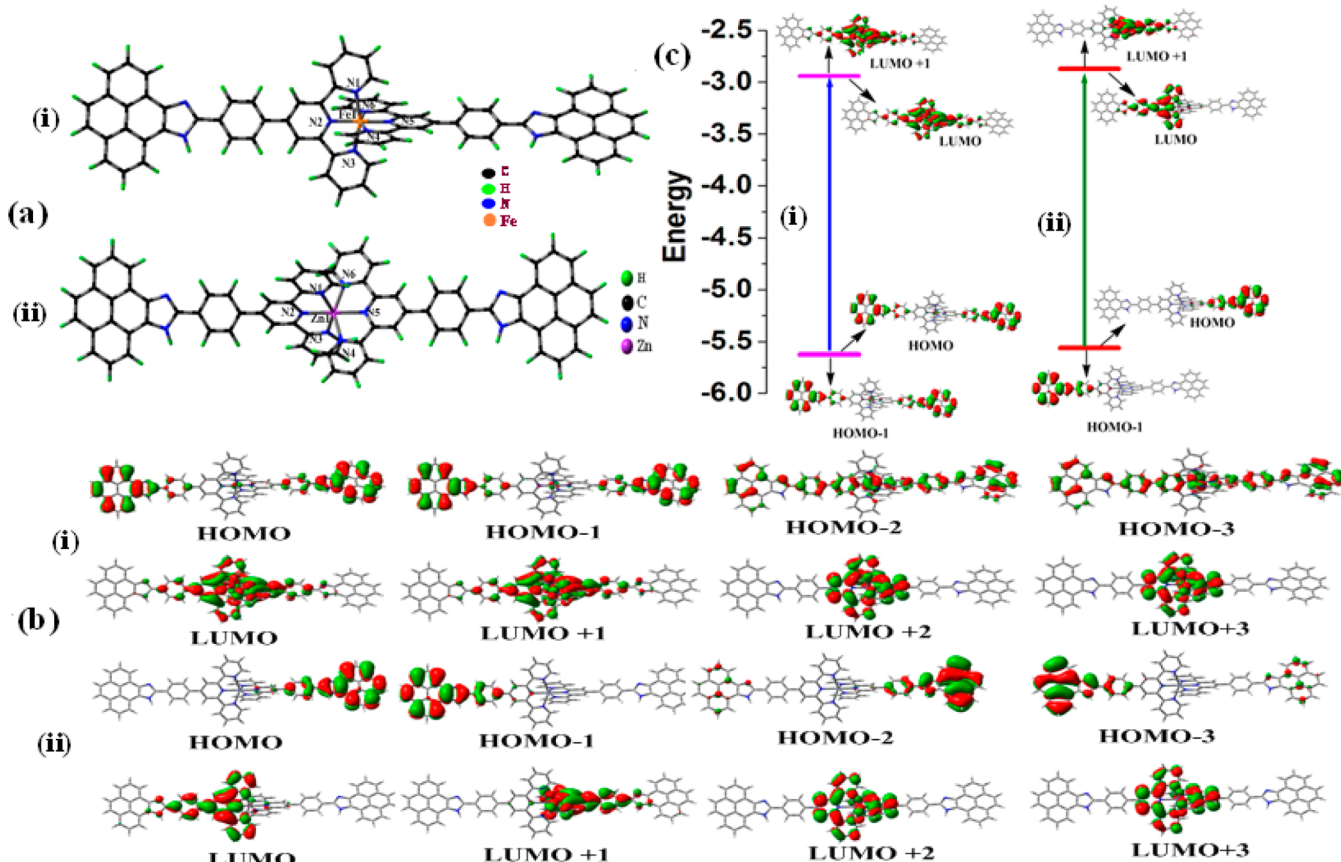


Figure 7. (a) Ground-state optimized geometries, (b) schematic drawings of the selective frontier molecular orbitals, and (c) energy level diagram depicting the dominant transitions that comprise the lowest-energy absorption band of $[Fe(\text{tpy-HImzPy})_2]^{2+}$ (i) and $[Zn(\text{tpy-HImzPy})_2]^{2+}$ (ii) in dimethyl sulfoxide.

addition of metal ion show that spectral saturation occurs upon addition of 0.5 equiv of metal ion in all cases, indicating the formation of a $[\text{M}(\text{tpy-HImzPy})_2]^{2+}$ complex (Figures S12–S18, Supporting Information). The presence of a peak at $m/z = 577.17$ for Fe^{2+} and $m/z = 581.57$ for Cu^{2+} in the ESI-MS spectrum also confirms the composition (Figures S19 and S20, Supporting Information). The UV-vis absorption and emission titration data were again utilized to derive the equilibrium constants (K) for the binding between tpy-HImzPy and the cations (Table 2). The red shift of the absorption band in the presence of the metal ions could be attributed to the metal-induced intraligand charge-transfer (ILCT) process from the pyrenyl-imidazole group to the tpy moiety. On the basis of the absorption and emission titrations, the detection limits of tpy-HImzPy for Fe^{2+} were found to be 2.59×10^{-9} and 2.81×10^{-9} M, respectively (Figures S21 and S22, Supporting Information). More importantly, tpy-HImzPy can also be applied for sensing in mixed 1:1 aqueous–organic (water–dimethyl sulfoxide) media (Figure S23, Supporting Information), making the receptor useful for practical applications.

Figure S24 (Supporting Information) shows the ^1H NMR spectra of free tpy-HImzPy as well as tpy-HImzPy in the presence of 0.5 equiv of Fe^{2+} in $\text{DMSO}-d_6$. It is evident that the H_3 proton of the tpy moiety is significantly affected because this proton experiences maximum shielding due to the anisotropic ring current effect of the adjacent pyridine of the other ligand. The other tpy protons (H_3' and H_6) get shifted to the downfield region. Again, as expected, the chemical shifts of the the pyrenyl-imidazole protons are almost invariant on metal coordination.

3.5. Computational Studies. The geometries of tpy-HImzPy, its NH deprotonated form (tpy-ImzPy), and three cationic adducts of composition $[\text{M}(\text{tpy-HImzPy})_2]^{2+}$ (where $\text{M} = \text{Fe}^{2+}, \text{Cu}^{2+}$, and Zn^{2+}) were optimized by the Gaussian 09 program and the optimized geometries for the compounds computed in dimethyl sulfoxide medium are presented in Figure 7a and Figures S25 and S26 (Supporting Information). The geometrical parameters are summarized in Tables S4 and S5, (Supporting Information). In the optimized structure of each metal complex, it is evident that the bivalent metal ion is coordinated in bis-tridentate fashion having a distorted octahedral geometry. The $\text{M}-\text{N}$ distances lie in the range between 1.905(7) and 2.256(7) Å, whereas the chelate bite angles span the range between 73.9 and 94.4°. Similar $\text{M}-\text{N}$ bond distances have also been observed for the reported bis-terpyridine metal complexes.⁴³ It is of interest to note that the central $\text{M}-\text{N}_{\text{py}}$ bond is shorter than the two outer $\text{M}-\text{N}_{\text{py}}$ bonds, probably because of efficient overlap of the metal t_{2g} orbital with the π^* orbitals of the central pyridyl group.

The frontier orbitals of $[\text{M}(\text{tpy-HImzPy})_2]^{2+}$ (where $\text{M} = \text{Fe}^{2+}$ and Zn^{2+}) are shown in Figure 7b, whereas those of tpy-HImzPy and tpy-ImzPy and $[\text{Cu}(\text{tpy-HImzPy})_2]^{2+}$ are presented in Figures S27 and S28 (Supporting Information). The orbital energies and compositions in terms of atomic contributions are reported in Tables S6–S8 (Supporting Information). It appears that the three highest occupied MOs (HOMO, HOMO-1, and HOMO-2) of tpy-HImzPy are mainly pyrenyl-imidazole in character, but some contributions also come from the phenyl as well as terpyridine moieties, whereas the lowest unoccupied MOs

Table 3. Selected UV–Vis Energy Transitions at the TD-DFT/B3LYP Level for tpy-HImzPy and tpy-ImzPy in Dimethyl Sulfoxide

excited state	$\lambda_{\text{cal}}/\text{nm}$ ($\epsilon_{\text{cal}}/\text{M}^{-1} \text{cm}^{-1}$), energy/eV	oscillator strength (f)	$\lambda_{\text{expt}}/\text{nm}$ ($\epsilon_{\text{expt}}/\text{M}^{-1} \text{cm}^{-1}$), energy/eV	key transitions
tpy-HImzPy				
S ₁	410 (40138), 3.02	0.81	394 (32980), 3.15	H → L (97%)
S ₅	338 (47312), 3.69	0.76	356 (38890), 3.48	H-1 → L (34%), H → L+3 (35%), H → L+4 (12%)
S ₂₅	261 (55079), 4.74	0.25	294 (54890), 4.22	H-2 → L+3 (53%), H-1 → L+3 (21%)
tpy-ImzPy				
S ₁	468 (38540), 2.65	0.74	428 (36100), 2.89	H → L (99%)
S ₇	330 (39560), 3.76	0.41	323 (32400), 3.84	H-1 → L+2 (11%), H → L+4 (35%), H → L+6 (47%)
S ₃₁	265 (64820), 4.68	0.56	258 (96250), 4.81	H-6 → L+1 (71%), H-9 → L+1 (8%)

(LUMO, LUMO+1, and LUMO+3) are essentially based on π^* orbitals of the terpyridine moieties. Calculations indicate that there are subtle differences in the compositions and shapes of the different frontier orbital between tpy-HImzPy and tpy-ImzPy and also between tpy-HImzPy and $[\text{M}(\text{tpy-HImzPy})_2]^{2+}$ where $\text{M} = \text{Fe}^{2+}$, Cu^{2+} , and Zn^{2+}). It is of interest to note that on going from tpy-HImzPy to $[\text{M}(\text{tpy-HImzPy})_2]^{2+}$, the contribution of the pyrenyl-imidazole moiety in HOMO, HOMO-1, and HOMO-2 decreases, whereas HOMO-3 increases slightly in all three cases. On the other hand, the terpyridine contribution increases in all the four LUMOs in $[\text{M}(\text{tpy-HImzPy})_2]^{2+}$ where $\text{M} = \text{Fe}^{2+}$, Cu^{2+} , and Zn^{2+}). It is worth noting that there is a very small but finite contribution of metal ions in the HOMOs of $[\text{M}(\text{tpy-HImzPy})_2]^{2+}$.

Time-dependent DFT calculations were performed to gain deeper insight into the electronic properties of the transitions involved in the absorption and emission processes.^{66–68} Utilizing the ground-state optimized geometries, we have computed the UV–vis absorption spectra of the compounds by TD-DFT approach. The calculated absorption energies associated with their oscillator strengths, the main configurations, are summarized in Tables 3 and 4 and Table S9 (Supporting Information). Figure 7c and Figures S29 and S30 (Supporting Information) display the energy levels of different molecular orbitals involved in the electronic transition process of the compounds. Figures S31–S33 (Supporting Information) present the combined experimental and simulated UV–vis spectra of the compounds. A good agreement between the vertical excitation energies and wavelengths of the absorption maxima in the experimental spectra was found, which allows us to assign the experimentally observed band. For example, the calculated absorption bands are obtained at 410, 338, and 261 nm for tpy-HImzPy. Taking into consideration the compositions of HOMOs and LUMOs involved in the transition processes, it can be concluded that the bands at 410 and 338 nm are due to an intraligand-charge-transfer transition (ILCT) and mainly involve a charge transfer from pyrenyl-imidazole moiety to the terpyridine unit of tpy-HImzPy. Again, the calculated absorption band at 261 nm is principally due to the transitions between π orbitals localized on pyrenyl-imidazole and terpyridine units. Moreover, the experimentally observed red shift of the low-energy ILCT bands when going from tpy-HImzPy to tpy-ImzPy and also from tpy-HImzPy to $[\text{M}(\text{tpy-HImzPy})_2]^{2+}$ (where $\text{M} = \text{Fe}^{2+}$, Cu^{2+} , and Zn^{2+}) is well reproduced from our calculations. Again, considering the compositions of the HOMOs and LUMOs involved in the absorption processes, the calculated lowest energy bands at 532, 528, and 518 nm for Fe^{2+} , Cu^{2+} , and Zn^{2+} complexes, respectively, can again be assigned as ILCT from the pyrenyl-imidazole group to the tpy moiety of coordinated tpy-HImzPy. However, the corresponding experimentally

observed bands at 585, 430, and 405 nm are not in good agreement with the calculated values (Figures S32 and S33 and Tables 4 and S9, Supporting Information). Although it is expected that the band at 585 nm is due to $\text{Fe}^{2+}(\text{d}\pi)-\pi^*(\text{tpy-HImzPy})$ MLCT, TD-DFT calculations shows the calculated band at 532 nm is predominantly ILCT character with a very minor contribution from MLCT.

The lowest singlet excited states S₁ of tpy-HImzPy and tpy-ImzPy were also optimized in the solution state by TD-DFT methodology, and selected geometrical parameters and their optimized structures are depicted in Figure S34 and Table S10 (Supporting Information), respectively. The calculated results reveal that geometrical parameters of the compounds have small differences from the ground-state structures. The emission energies of tpy-HImzPy and tpy-ImzPy were calculated by optimizing their singlet excited-state geometries (Table S11, Supporting Information). The frontier orbitals of tpy-HImzPy and tpy-ImzPy in the singlet excited state are presented in Figure S35 (Supporting Information). The plots of frontier molecular orbitals related to emissions of the compounds are presented in Figure S36 (Supporting Information). According to TD-DFT calculations, the emission bands were obtained at 494 and 560 nm, for tpy-HImzPy and tpy-ImzPy, respectively (Table S11, Supporting Information). The corresponding experimental values obtained at 507 and 568 nm for tpy-HImzPy and tpy-ImzPy nicely correlate with the computed values. The ILCT nature of the emission in both tpy-HImzPy and tpy-ImzPy was also verified by analyzing the composition of HOMOs and LUMOs in the excited state of both compounds. Moreover, the trend of the experimentally observed red shift of emission maximum on going from tpy-HImzPy to tpy-ImzPy is also reproduced by the calculated results.

3.6. Molecular Logic Operations. The sensing studies inspire us to utilize tpy-HImzPy for performing several logic functions by sequential use of two ionic inputs such as Fe^{2+} and F^- , and Cu^{2+} and CN^- , and monitoring either absorbance or luminescence as the output. The INHIBIT gate interpreted as a particular integration of AND and NOT logic gates deserves attention because of its noncommutative behavior, meaning the output signal is inhibited by only one powerful input. To examine INHIBIT logical behavior of tpy-HImzPy with Fe^{2+} and F^- inputs, the absorbance at 585 nm was monitored as the output signal. The increase in absorbance, i.e., output, was found to be high only with Fe^{2+} as an input (Input 1), which is equivalent to a YES operation. The output is low in the presence of F^- (Input 2), thereby implementing the necessity of a NOT gate. But in the presence of both inputs, the output signal is again low, contradicting the function of an AND gate. Here the increase in absorbance value in the presence of input 1 will be hindered by the presence of input 2. Thus, the observations along with the

Table 4. Selected UV–Vis Energy Transitions at the TD-DFT/B3LYP Level of $[\text{Fe}(\text{tpy-HImzPy})_2]^{2+}$ and $[\text{Zn}(\text{tpy-HImzPy})_2]^{2+}$ in Dimethyl Sulfoxide

excited state	$\lambda_{\text{cal}}/\text{nm}$ ($\epsilon_{\text{cal}}/\text{M}^{-1}\text{ cm}^{-1}$), energy/eV	oscillator strength (f)	$\lambda_{\text{exp}}/\text{nm}$ ($\epsilon_{\text{exp}}/\text{M}^{-1}\text{ cm}^{-1}$), energy/eV	key transitions
S_2	536 (51120), 2.31	1.20	585 (35750), 2.12	$[\text{Fe}(\text{tpy-HImzPy})_2]^{2+}$
S_{23}	381 (36900), 3.25	1.07	410 (35700), 3.02	$H-1 \rightarrow L+1$ (43%), $H \rightarrow L$ (50%), $H-3 \rightarrow L+1$ (2%), $H-2 \rightarrow L$ (3%)
S_{70}	311 (63350), 3.99	0.14	363 (sh) (44610), 3.42	$H-1 \rightarrow L+4$ (44%), $H- \rightarrow L+5$ (44%), $H-1 \rightarrow L+6$ (3%), $H \rightarrow L+7$ (3%)
S_{97}	288 (72500), 4.31	0.79	325 (69251), 3.81	$H-10 \rightarrow L+10$ (65%), $H-4 \rightarrow L+5$ (15%), $H-12 \rightarrow L$ (8%), $H-9 \rightarrow L+1$ (5%)
S_{179}	250 (47450), 4.96	0.14	288 (69120), 4.31	$H-10 \rightarrow L+2$ (26%), $H-9 \rightarrow L+3$ (13%), $H-14 \rightarrow L+2$ (8%), $H-13 \rightarrow L+3$ (8%), $H-11 \rightarrow L+3$ (2%), $H-8 \rightarrow L+7$ (4%), $H-6 \rightarrow L+7$ (7%), $H-5 \rightarrow L+6$ (7%)
S_1	518 (27800), 2.39	0.8901	405 (27650), 3.07	$[\text{Zn}(\text{tpy-HImzPy})_2]^{2+}$
S_9	350 (61100), 3.54	1.4040	341 (30600), 3.64	$H-1 \rightarrow L$ (52%), $H \rightarrow L+1$ (39%), $H-1 \rightarrow L+1$ (4%), $H \rightarrow L$ (4%)
S_{49}	291 (80970), 4.26	0.9638	290 (48000), 4.28	$H-3 \rightarrow L$ (15%), $H-2 \rightarrow L+1$ (11%), $H-1 \rightarrow L+4$ (30%), $H \rightarrow L+5$ (26%), $H-3 \rightarrow L+1$ (2%), $H-2 \rightarrow L$ (3%)
				$H-5 \rightarrow L+4$ (11%), $H-4 \rightarrow L+5$ (11%), $H-3 \rightarrow L+4$ (24%), $H-2 \rightarrow L+5$ (25%), $H-1 \rightarrow L+12$ (5%), $\text{HOMO} \rightarrow L+13$ (5%)

truth table compiled in Figure 8 can be correlated with the function of an INHIBIT gate.

Next, we will examine the XOR behavior of tpy-HImzPy by taking Cu^{2+} (0.5 equiv) and CN^- (3.0 equiv) as input 1 and input 2, respectively, and monitoring the absorbance at 430 nm. The XOR logic functions are based on “either/or” strategy. The output signal is in the on-state if either, but not both, of the inputs is in the on-state. The output is in the off-state if both inputs are in the on-state. In our case, the output is high in the presence of either Cu^{2+} or CN^- as input. Moreover, either in the presence or in the absence of two inputs, the output is low. This observation well matches with XOR logical behavior as shown in Figure 9.

Again, by variation of the amount of the inputs [Cu^{2+} (0.5 equiv) and CN^- (18.0 equiv)], tpy-HImzPy can mimic the function of an OR gate. The output of an OR gate is on-state when either one or both inputs are in the on-state. In the absence of both inputs, the absorbance at 430 nm of the receptor is low, i.e., in the off-state, whereas the absorbance is enhanced in the presence of each or both of the two inputs. Thus, the truth table in Figure 10 clearly indicates the behavior of a two-input OR logic gate. Moreover, sequential combination of Fe^{2+} and F^- inputs with absorbance at 428 nm as output can give rise to an OR logic function (Figure S37, Supporting Information).

Thus, far, we have utilized the absorbance at a specified wavelength as the output signal. To test the viability of tpy-HImzPy to mimic the function of XNOR gate, the combination of either Cu^{2+} (Input 1) and CN^- (Input 2) or Fe^{2+} (Input 1) and F^- (Input 2) can be taken as the inputs and the fluorescence intensity at 507 nm can be monitored as the output signal (Figure 11 and Figure S38 Supporting Information). In the presence of either input 1 or input 2, the fluorescence intensity of the receptor decreases dramatically, but conjugative addition of the inputs $\{\text{Cu}^{2+}$ (0.5 equiv) and CN^- (3.0 equiv) leads to significant enhancement of the fluorescence intensity. This observation correlates well with the function of an XNOR logic gate (Figure 11 and Figure S38 Supporting Information).

Finally, we again take the same ionic inputs and output as XNOR gate but vary the amount of the inputs [Cu^{2+} (0.5 equiv) and CN^- (18.0 equiv) or Fe^{2+} (0.5 equiv) and F^- (15.0 equiv)] to check the NOR gate behavior (Figure 12 and Figure S39 Supporting Information). A NOR gate, which integrates NOT and OR logic functions is a universal gate that allows the combinatorial creation of all other Boolean operations. It is evident that the output of the NOR gate is in the switched-on state only when both inputs are absent. In the presence of any of these inputs, the fluorescence intensity of the receptor is dramatically decreased, whereas in the absence of each or both of these two inputs, the fluorescence intensity is high. Thus, the observations clearly indicate a two-input NOR logic gate according to the truth table shown in Figure 12 and Figure S39 (Supporting Information).

The performance of different logic functions is based on coordination of metal ions such as Cu^{2+} and Fe^{2+} with the receptor followed by its reversible decoordination by CN^- and F^- , respectively. The effects of incremental addition of CN^- to $[\text{Cu}(\text{tpy-HImzPy})_2]^{2+}$ and F^- to $[\text{Fe}(\text{tpy-HImzPy})_2]^{2+}$ were monitored by both absorption and emission spectroscopic methods (Figure 13 and Figure S40, Supporting Information). On the basis of the two-step process in both cases, we propose that the first step is the decomplexation of metals (Cu^{2+} or Fe^{2+}) from $[\text{M}(\text{tpy-HImzPy})_2]^{2+}$ upon addition of 3 equiv of CN^- or F^- , giving rise to the free ligand and more stable cyanide and fluoride complexes of the metals. In the second step, addition of

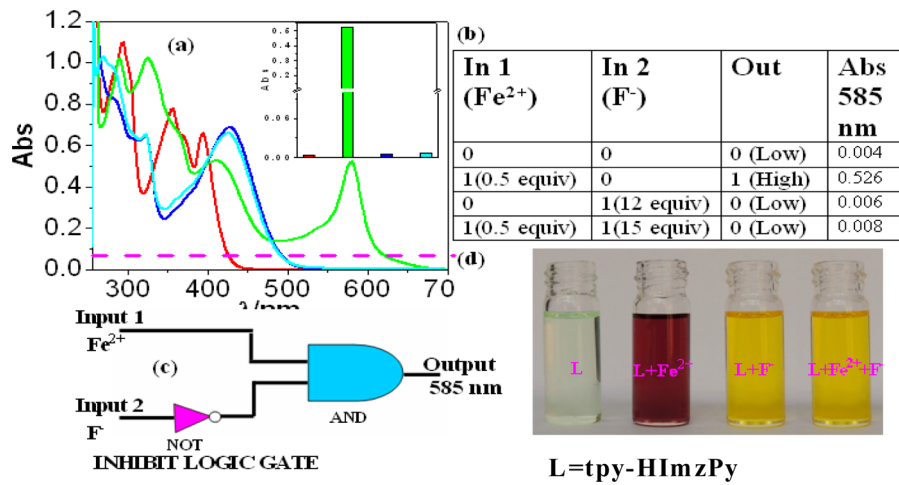


Figure 8. (a) INIHIBIT logic gate based on absorbance at 585 nm. The horizontal dotted line represents the threshold value. (b) Truth table. (c) Schematic representation of an INIHIBIT gate. (d) Photograph of L in dimethyl sulfoxide in the presence of different inputs.

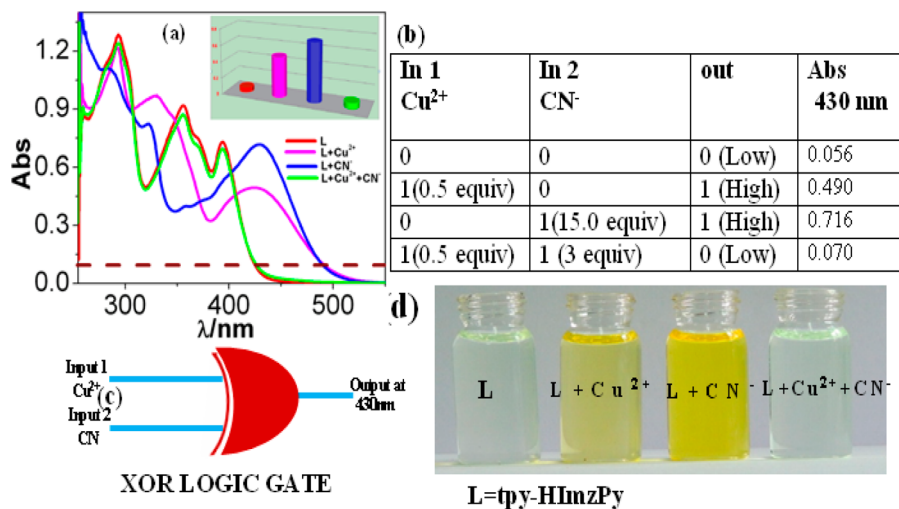


Figure 9. (a) XOR logic gate based on absorbance at 430 nm. The horizontal dotted line represents the threshold value. (b) Truth table. (c) Schematic representation of an XOR gate. (d) Photograph of L in dimethyl sulfoxide in the presence of different inputs.

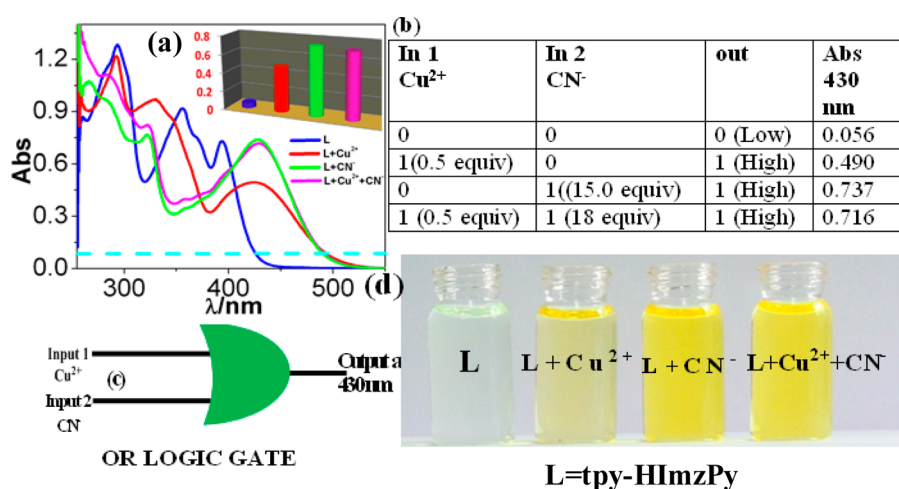


Figure 10. (a) OR logic gate based on absorbance at 430 nm. The horizontal dotted line represents the threshold value. (b) Truth table. (c) Schematic representation of an OR gate. (d) Photograph of L in dimethyl sulfoxide in the presence of different inputs.

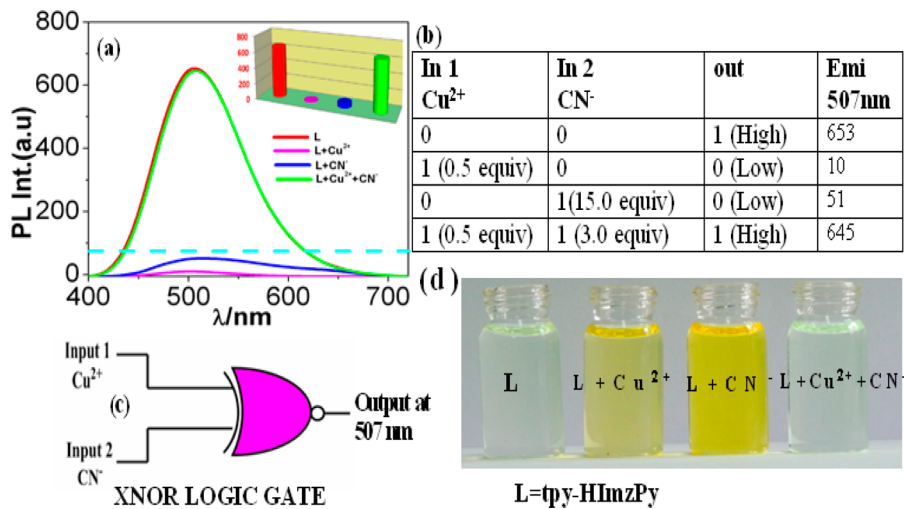


Figure 11. (a) XNOR logic gate based on emission at 507 nm. The horizontal dotted line represents the threshold value. (b) Truth table. (c) Schematic representation of an XNOR gate. (d) Photograph of L in dimethyl sulfoxide in the presence of different inputs.

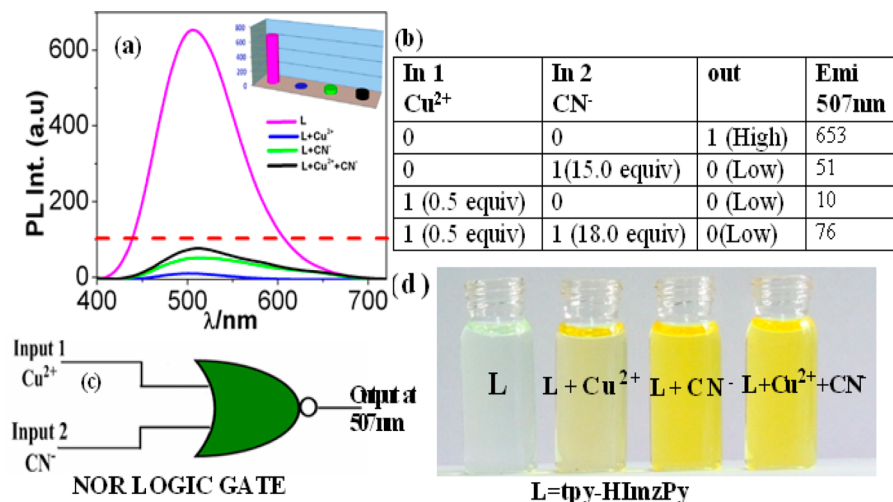


Figure 12. (a) NOR logic gate based on emission at 507 nm. The horizontal dotted line represents the threshold value. (b) Truth table. (c) Schematic representation of an NOR gate. (d) Photograph of L in dimethyl sulfoxide in the presence of different inputs.

excess CN⁻ or F⁻ leads to the deprotonation of the imidazole NH proton of tpy-HImzPy. Moreover, the reversibility of the spectral response toward successive coordination by Cu²⁺ and decoordination by CN⁻ was clearly demonstrated in Figure S41 (Supporting Information).

3.7. Fuzzy Logic Operations. Conversion of the multiply configurable Boolean logic element of the receptor to the desired system capable of carrying out Fuzzy logic, hereafter called a Fuzzy Inference Engine, is possible by switching from a digital-type to an analog-type addition of the chemical inputs. On the basis of the fuzzy nature of chemical reactions, the uncertain information in the analogue region can be addressed to implement soft computation through the formulation in Fuzzy Logic System (FLS).^{16–21} FLS consists of nonlinear mapping of input crisp data vector (\bar{x}) into scalar crisp output (y) and this mapping can be quantitatively represented by the function $y = f(\bar{x})$. As already been mentioned, four basic elements (fuzzifier, rules, inference engine, and defuzzifier) constitute the FLS. A fuzzy set S for the variable X , can be characterized by a membership function, $\mu_S(x)$, consisting of a real number, included in the interval [0, 1], to each element of X . Fuzzy variables are usually referred to as linguistic variables, such as the concentration of

the added ions and fluorescence quantum yield. In the absence of exact values of the variables, we designate the variable in terms of a few linguistic values such as low, medium, or high.

It has already been demonstrated that the fluorescence quantum yield of the receptor can be modulated to a significant extent through the external chemical inputs such as Fe²⁺, Cu²⁺, F⁻, and CN⁻. Figure 14 shows the change in fluorescence intensity (quantum yield) recorded after addition of different amounts of Fe²⁺ (with the molar ratio $n_{\text{Fe}}^{2+}/n_{\text{tpy-HImzPy}}$ ranging from 0 up to 0.5 equiv). The input variable (Fe²⁺) and output variable (emission quantum yield, Φ) have been defined by the fuzzy sets, as shown in Figure 14. The inference rules, which are expressed as a collection of IF-THEN statements, can be taken from blue box of Figure 14. Typical example of IF-THEN statements: IF Fe²⁺ is low, THEN quantum yield is high. The IF part is designated as the antecedent, and the THEN part is called the consequence. The inference engine of the FLS then maps the input fuzzy sets into the output fuzzy sets. The defuzzifier maps the output fuzzy sets into crisp numbers. The output crisp number can lead to the prediction of a variable, like quantum yield, Φ . Similarly, the fuzzy relation based on fuzzy interference

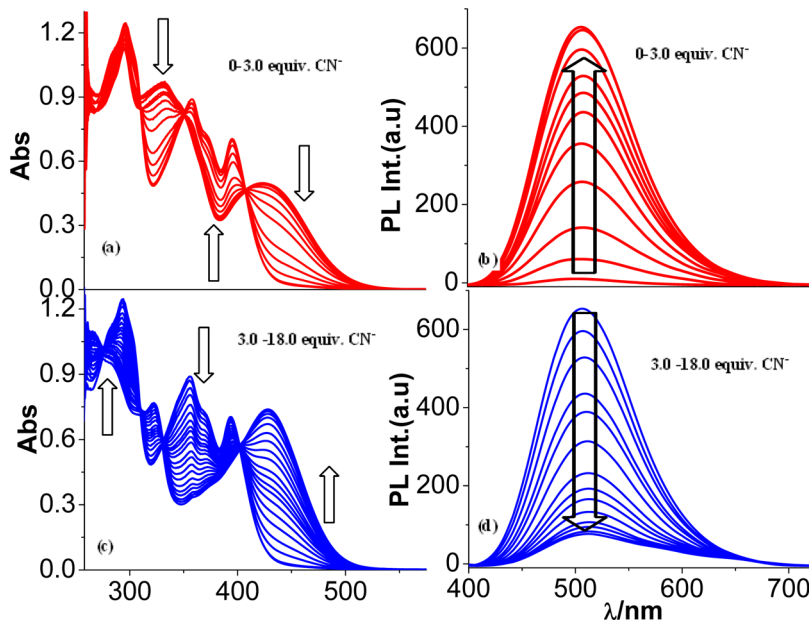


Figure 13. Change in UV–vis absorption (a and c) and photoluminescence (b and d) spectrum of $[\text{Cu}(\text{tpy-HImzPy})_2]^{2+}$ in dimethyl sulfoxide upon incremental addition of CN^- .

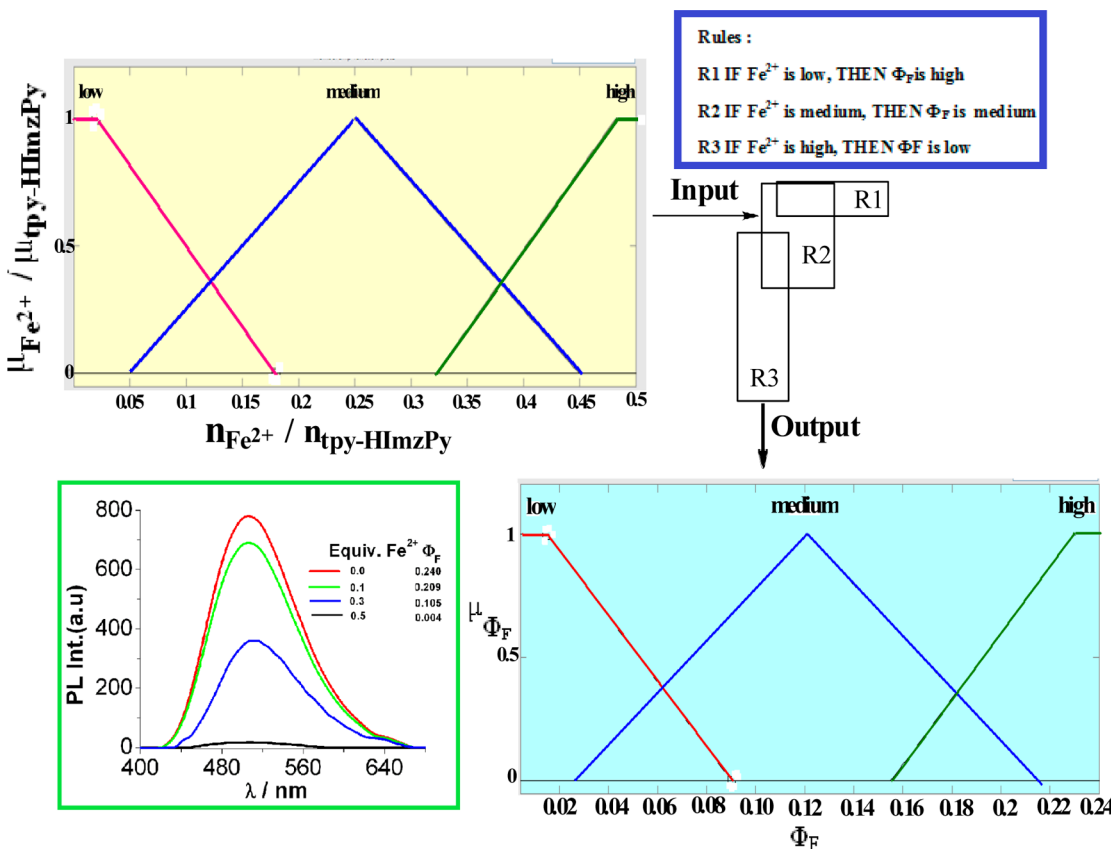


Figure 14. Schematic presentation of fuzzy relation based on fuzzy inference rules taking Fe^{2+} as input and the emission quantum yield (Φ_F) as the output. The change of emission intensity of tpy-HImzPy as a function of Fe^{2+} is represented in the green box. Fuzzy variables are decomposed in three fuzzy sets. Fe^{2+} : (1) low (zmf μ_{low} [0.036 0.164]); (2) medium (trimf μ_{medium} [0.05 0.25 0.45]); (3) high (smf μ_{high} [0.336 0.464]). Φ_F : (1) low (zmf μ_{low} [0.013 0.088]); (2) medium (trimf μ_{medium} [0.027 0.122 0.216]); (3) high (smf μ_{high} [0.155 0.231]).

rule mapping out input F^- and output emission quantum yield is presented in Figure S42 (Supporting Information).

Now we will be interested to see the effects of simultaneous injection of two chemical inputs into the solution of the receptor

on its emission intensity as well as the quantum yield. Addition of Cu^{2+} to the receptor solutions decrease the fluorescence intensities but simultaneous addition of Cu^{2+} and CN^- may either increase or decrease the intensities (Figure S43 and

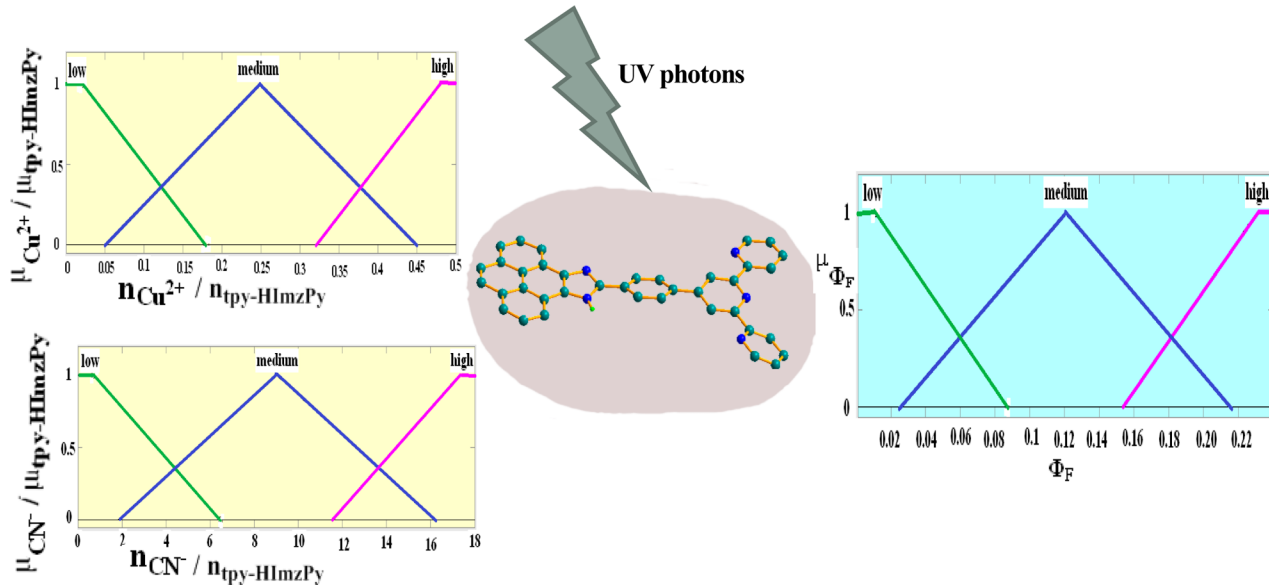


Figure 15. Fuzzy logic system based on the fluorogenic behavior of tpy-HImzPy by adopting Mamdani's method.⁵² The mole ratios $n_{\text{Cu}^{2+}}/\text{n}_{\text{tpy-HImzPy}}$ and $n_{\text{CN}^-}/\text{n}_{\text{tpy-HImzPy}}$ act as inputs, and the quantum yield (Φ_F) of tpy-HImzPy plays the role of output. All the variables are decomposed into three fuzzy sets labeled as low, medium, and high.

Table S12, Supporting Information). Therefore, the fluorogenic receptor can be exploited to implement Fuzzy logic functions with UV radiation as power supply, varying amount of Cu^{2+} and CN^- as the chemical inputs, and fluorescence quantum yield as the outputs (Figure 15). In FLS, the rules are “IF ... , THEN ...” statements with multiple antecedents involving the OR, AND operators. With different probable combinations of Cu^{2+} and CN^- , 13 rules are listed in Table S13 (Supporting Information). Here, the mole ratio of Cu^{2+} and tpy-HImzPy ($n_{\text{Cu}^{2+}}/\text{n}_{\text{tpy-HImzPy}}$) can be decomposed into three fuzzy sets: (1) low, with a membership function (μ_L) whose symbol will be zmf [0.02 0.18] and is situated to the left of the diagram, (2) medium, with membership function μ_M and having a triangular shape function bearing the symbol trimf [0.05 0.25 0.45], and (3) high, with membership function (μ_H), which is open to the right and whose symbol will be smf [0.36 0.48]. The other input variable, CN^- , can also be decomposed into three fuzzy sets: (1) low (with a zmf μ_L , [0.723 6.8]; (2) medium (with a trimf μ_M , [1.8 9 16.2]; (3) high (with a smf μ_H , [11.52 17.28]). The output variable, Φ_F , will also be categorized into three fuzzy sets: (1) low (with a zmf μ_L , [0.010 0.087]); (2) medium (with a trimf μ_M , [0.025 0.120 0.216]; (3) high (with a smf μ_H , [0.154 0.230]). A schematic representation of the fuzzy sets involving all the variables is shown in Figure 15. Our next task to implement Mamdani's FLS entails formulating fuzzy rules.⁵² Fuzzy rules have already been described to be IF-THEN statements, wherein the IF part is called the antecedent, and the THEN part is called the consequence. Due to the synergistic action of both inputs, the dual antecedents are connected here through the OR and AND operators. The entire collection of fuzzy rules encompassing both OR and AND operators is summarized in Table S13 (Supporting Information) and a three-dimensional representation of the dependence of emission quantum yield of the receptor as a function of simultaneous injection of two chemical inputs (Cu^{2+} and CN^-) is portrayed in Figure 16.

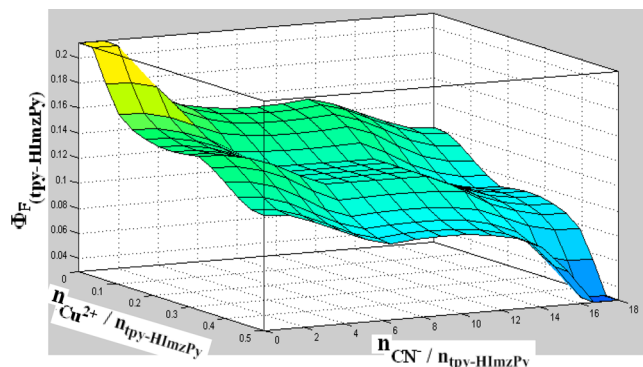


Figure 16. Three-dimensional representation of the dependence of emission quantum yield of tpy-HImzPy ($\Phi_F(\text{tpy-HImzPy})$) as a function of simultaneous injection of two chemical inputs (Cu^{2+} and CN^-).

4. CONCLUSIONS

We are interested in studying molecular systems whereby the change in optical properties by interaction with selective anions and cations can be utilized for the construction of molecular logic gates. In this context, we have presented a combined experimental and theoretical study of a pyrene–phenylimidazole–terpyridine conjugate. On the experimental side, the effect of anions and cations on the photophysical properties of tpy-HImzPy was thoroughly investigated. To gain a better understanding of the electronic structure and excited-state properties, we have carried out DFT and TDDFT calculations on tpy-HImzPy and its selected anionic and cationic adducts. The good correlation between the experimental and the TD-DFT calculated absorption and emission spectral behaviors allowed us to provide a detailed assignment of the main spectral features of the investigated compounds. More importantly, on the basis of the response profiles of tpy-HImzPy in terms of absorption or emission intensity and wavelength toward selected cationic and anionic guests, we developed a unique molecular system capable of performing five independent logic functions such INHIBIT, OR, XOR, NOR, and XNOR. In addition, Fuzzy logic can also be

implemented into the present system. The Fuzzy logic computing is thought to be a potential alternative in utilizing the vague nature of chemical reactions for modeling the imprecise modes of reasoning and sensing. Thus, the present system on which both Boolean and Fuzzy logic operations have been implemented will be of importance for applications in molecular computation and in artificial intelligence.

■ ASSOCIATED CONTENT

§ Supporting Information

Structural parameters (crystal data, bond distances and angles) along with figures and tables related to molecular structures, molecular orbitals, ESI mass, NMR, UV-vis absorption, steady-state and time-resolved luminescence spectral change as a function of different ions, energy level diagrams, DFT and TD-DFT calculations, OR, XNOR, and NOR logic gates, and the fuzzy relation (Figures S1–S44 and Table S1–S13). This material is available free of charge via the Internet at <http://pubs.acs.org>.

■ AUTHOR INFORMATION

Corresponding Author

*S. Baitalik. E-mail: sbaitalik@hotmail.com. Telephone: 91-033-2414-6666.

Notes

The authors declare no competing financial interest.

■ ACKNOWLEDGMENTS

We gratefully acknowledge the financial support from CSIR and DST, Government of India through project 01(2766)/13/EMR-II and SR/S1/IC-33/2010, respectively. The authors thank Dr. Ajay Kumar Mishra of the Department of Chemistry & Chemical Technology of Vidyasagar University for his valuable input in the area of DFT and TD-DFT computation. S.K. and D.M are grateful to CSIR and S.M. is grateful to UGC for their fellowship.

■ REFERENCES

- (1) de silva, A. P.; Gunaratne, H. Q. N.; McCoy, C. P. A molecular photoionic AND gate based on fluorescent signaling. *Nature* **1993**, *364*, 42–44.
- (2) de Silva, A. P.; Gunaratne, H. Q. N.; Maguire, G. E.M. ‘Off-on’ fluorescent sensors for physiological levels of magnesium ions based on photoinduced electron transfer (PET), which also behave as photoionic OR logic gates. *J. Chem. Soc., Chem. Commun.* **1994**, 1213–1214.
- (3) de Silva, A. P.; Gunaratne, H. Q. N.; McCoy, C. P. Molecular photoionic AND logic gates with bright fluorescence and “off-on” digital action. *J. Am. Chem. Soc.* **1997**, *119*, 7891–7892.
- (4) de Silva, A. P.; McClenaghan, N. D. Molecular-scale Logic Gates. *Chem.—Eur. J.* **2004**, *10*, 574–586.
- (5) de Silva, A. P. Molecular logic gate arrays. *Chem.—Asian J.* **2011**, *6*, 750–766.
- (6) Ben-Ari, M. *Mathematical logic for computer science*; Prentice-Hall: Hemel Hempstead, 1993.
- (7) Mitchell, R. J. *Microprocessor Systems: An Introduction*; Macmillan: London, 1995.
- (8) Katz, E. (Ed.) *Molecular and Supramolecular Information Processing: From Molecular Switches to Logic Systems*; Wiley-VCH: Weinheim, Germany, 2012.
- (9) Raymo, F. M. Digital processing and communication with molecular switches. *Adv. Mater.* **2002**, *14*, 401–414.
- (10) Gust, D.; Andréasson, J.; Pischel, U.; Moore, T. A.; Moore, A. L. Data and signal processing using photochromic molecules. *Chem. Commun.* **2012**, *48*, 1947–1957.
- (11) Ball, P. Chemistry meets computing. *Nature* **2000**, *406*, 118–120.
- (12) de Ruiter, G.; van der Boom, M. E. Surface-confined assemblies and polymers for molecular logic. *Acc. Chem. Res.* **2011**, *44*, 563–573.
- (13) Andréasson, J.; Pischel, U. Smart molecules at work mimicking advanced logic operations. *Chem. Soc. Rev.* **2010**, *39*, 174–188.
- (14) Credi, A. Molecules that make decisions. *Angew. Chem., Int. Ed.* **2007**, *46*, 5472–5475.
- (15) Sreejith, S.; Ajayaghosh, A. Molecular logic gates: Recent advances and perspectives. *Indian J. Chem.* **2012**, *S1A*, 47–56.
- (16) Gentili, P. L. The fundamental Fuzzy logic operators and some complex Boolean logic circuits implemented by the chromogenism of a spirooxazine. *Phys. Chem. Chem. Phys.* **2011**, *13*, 20335–20344.
- (17) Gentili, P. L. Boolean and Fuzzy logic gates based on the interaction of flindersine with bovine serum albumin and tryptophan. *J. Phys. Chem. A* **2008**, *112*, 11992–11997.
- (18) Gentili, P. L. Molecular processors: from qubits to Fuzzy logic. *ChemPhysChem.* **2011**, *12*, 739–745.
- (19) Gentili, P. L. Boolean and fuzzy logic implemented at the molecular level. *Chem. Phys.* **2007**, *336*, 64–73.
- (20) Gentili, P. L. The fuzziness of a chromogenic spirooxazine. *Dyes Pigments.* **2014**, *110*, 235–248.
- (21) Huang, W. T.; Luo, H. Q.; Li, N. B. Boolean logic tree of graphene-based chemical system for molecular computation and intelligent molecular search query. *Anal. Chem.* **2014**, *86*, 4494–4500.
- (22) Magri, D. C.; Fava, M. C.; Mallia, C. J. A sodium-enabled ‘Pourbaix sensor’: a three-input AND logic gate as a ‘lab-on-a-molecule’ for monitoring Na^+ , pH and pE. *Chem. Commun.* **2014**, *50*, 1009–1011.
- (23) Kumar, M.; Kumar, R.; Bhalla, V. ‘On–Off’ reversible switch for Fe^{3+} and F^- mimicking XNOR logic function. *Tetrahedron Lett.* **2010**, *S1*, 5559–5562.
- (24) Mahato, P.; Saha, S.; Das, A. Rare example of TICT based optical responses for the specific recognition of Cr^{3+} by a 2,2':6',2"-terpyridine derivative and demonstration of multiple logic operations. *J. Phys. Chem. C* **2012**, *116*, 17448–17457.
- (25) Ajayakumar, M. R.; Hundalb, G.; Mukhopadhyay, P. A tetrastable naphthalenediimide: anion induced charge transfer, single and double electron transfer for combinational logic gates. *Chem. Commun.* **2013**, *49*, 7684–7686.
- (26) Pischel, U.; Uzunova, V. D.; Remo, P.; Nau, W. M. Supramolecular logic with macrocyclic input and competitive reset. *Chem. Commun.* **2010**, *46*, 2635–2637.
- (27) Li, A.-F.; Ruan, Y.-B.; Jiang, Q.-Q.; He, W.-B.; Jiang, Y.-B. Molecular logic gates and switches based on 1,3,4-Oxadiazoles Triggered by Metal Ions. *Chem.—Eur. J.* **2010**, *16*, 5794–5802.
- (28) Miyaji, H.; Kim, H.-K.; Sim, E.-K.; Lee, C.-K.; Cho, W.-S.; Sessler, J. L.; Lee, C.-H. Coumarin-Strapped Calix[4]pyrrole: A fluorogenic anion receptor modulated by cation and anion binding. *J. Am. Chem. Soc.* **2005**, *127*, 12510–12512.
- (29) Credi, A.; Balzani, V.; Langford, S. J.; Stoddart, J. F. Logic operations at the molecular level. an XOR gate based on a molecular machine. *J. Am. Chem. Soc.* **1997**, *119*, 2679–2681.
- (30) Meng, X.; Zhu, W.; Zhang, Q.; Feng, Y.; Tan, W.; Tian, H. Novel bis(heterocyclic)ethenes containing a biphenylidene as the center ethene bridge: photochromism and solvatochromism for combined NOR and INHIBIT logic gates. *J. Phys. Chem. B* **2008**, *112*, 15636–15645.
- (31) de Silva, A. P.; Dixon, I. M.; Gunaratne, H. Q. N.; Gunnlaugsson, T.; Maxwell, P. R. S.; Rice, T. E. Integration of logic functions and sequential operation of gates at the molecular-scale. *J. Am. Chem. Soc.* **1999**, *121*, 1393–1394.
- (32) Bozdemir, O. A.; Guliyev, R.; Buyukcakir, O.; Selcuk, S.; Kolemen, S.; Gulseren, G.; Nalbantoglu, T.; Boyaci, H.; Akkaya, E. U. Selective manipulation of ICT and PET processes in styryl-bodipy derivatives: applications in molecular logic and fluorescence sensing of metal ions. *J. Am. Chem. Soc.* **2010**, *132*, 8029–8036.
- (33) Gotor, R.; Costero, A. M.; Gil, S.; Parra, M.; Gavin, P.; Rurack, K. Boolean operations mediated by an ion-pair receptor of a multi-readout molecular logic gate. *Chem. Commun.* **2013**, *49*, 11056–11058.
- (34) Margulies, D.; Melman, G.; Felder, C. E.; Arad-Yellin, R.; Shanzer, A. Chemical input multiplicity facilitates arithmetical processing. *J. Am. Chem. Soc.* **2004**, *126*, 15400–15401.

- (35) Komatsu, H.; Matsumoto, S.; Tamaru, S.; Kaneko, K.; Ikeda, M.; Hamachi, I. Supramolecular hydrogel exhibiting four basic logic gate functions to fine-tune substance release. *J. Am. Chem. Soc.* **2009**, *131*, 5580–5585.
- (36) Bhowmik, S.; Das, R. N.; Parasarb, B.; Dash, J. pH dependent multifunctional and multiconfigurable logic gate systems based on small molecule G-quadruplex DNA recognition. *Chem. Commun.* **2013**, *49*, 1817–1819.
- (37) Zhai, W.; Du, C.; Li, X. A series of logic gates based on electrochemical reduction of Pb^{2+} in self-assembled G-quadruplex on the gold electrode. *Chem. Commun.* **2014**, *50*, 2093–2095.
- (38) Zou, Q.; Li, X.; Zhang, J.; Zhou, J.; Sun, B.; Tian, H. Unsymmetrical diarylethenes as molecular keypad locks with tunable photochromism and fluorescence via Cu^{2+} and CN^- coordinations. *Chem. Commun.* **2012**, *48*, 2095–2097.
- (39) Andréasson, J.; Pischel, U.; Straight, S. D.; Moore, T. A.; Moore, A. L.; Gust, D. All-photonic multifunctional molecular logic device. *J. Am. Chem. Soc.* **2011**, *133*, 11641–11648.
- (40) Chen, S.; Yang, Y.; Wu, Y.; Tian, H.; Zhu, W. Multi-addressable photochromic terarylene containing benzo[*b*]thiophene-1,1-dioxide unit as ethene bridge: multifunctional molecular logic gates on unimolecular platform. *J. Metr. chem.* **2012**, *22*, 5486–5494.
- (41) Xue, P.; Lu, R.; Jia, J.; Takafuji, M.; Ihara, H. A Smart gelator as a chemosensor: application to integrated logic gates in solution, gel, and film. *Chem.—Eur. J.* **2012**, *18*, 3549–3558.
- (42) Saha, D.; Das, S.; Karmakar, S.; Dutta, S.; Baitalik, S. Synthesis, structural characterization and anion-, cation- and solvent-induced tuning of photophysical properties of a bimetallic Ru(II) complex: combined experimental and DFT/TDDFT investigation. *RSC Adv.* **2013**, *3*, 17314–17334.
- (43) Bhaumik, C.; Das, S.; Maity, D.; Baitalik, S. A terpyridyl-imidazole (tpy-HImzPh₃) based bifunctional receptor for multichannel detection of Fe^{2+} and F^- ions. *Dalton Trans.* **2011**, *40*, 11795–11808.
- (44) Bhaumik, C.; Saha, D.; Das, S.; Baitalik, S. Synthesis, structural characterization, photophysical, electrochemical, and anion-sensing studies of luminescent homo- and heteroleptic ruthenium(II) and osmium(II) complexes based on terpyridyl-imidazole ligand. *Inorg. Chem.* **2011**, *50*, 12586–12600.
- (45) Maity, D.; Das, S.; Mardanya, S.; Baitalik, S. Synthesis, structural characterization, and photophysical, spectroelectrochemical, and anion-sensing studies of heteroleptic ruthenium(II) complexes derived from 4'-Polyaromatic-Substituted terpyridine derivatives and 2,6-bis-(benzimidazol-2-yl)pyridine. *Inorg. Chem.* **2013**, *52*, 6820–6838.
- (46) Maity, D.; Bhaumik, C.; Mondal, D.; Baitalik, S. Ru(II) and Os(II) complexes based on terpyridyl-imidazole ligand rigidly linked to pyrene: synthesis, structure, photophysics, electrochemistry, and anion-sensing studies. *Inorg. Chem.* **2013**, *52*, 13941–13955.
- (47) Nakamaru, K. *Bull. Chem. Soc. Jpn.* **1982**, *55*, 1639–1640.
- (48) SAINT (version 6.02), SADABS (version 2.03); Bruker AXS Inc.: Madison, WI, 2002.
- (49) Sheldrick, G. M. *SHELXL-97, Program for the Refinement of crystal Structures*; University of Göttingen: Göttingen, Germany, 1997.
- (50) SHELXTL (version 6.10); Bruker AXS Inc.: Madison, WI, 2002.
- (51) Zadeh, L. A. *IEEE Software* **1994**, *11*, 48–56.
- (52) Mamdani, E. H. *IEEE Trans. Comput.* **1977**, *26*, 1182–1191.
- (53) Frisch, M. J.; Trucks, G. W.; Schlegel, H. B.; Scuseria, G. E.; Robb, M. A.; Cheeseman, J. R.; Scalmani, G.; Barone, V.; Mennucci, B.; Petersson, G. A.; et al. *Gaussian 09*, revision A.02; Gaussian Inc.: Wallingford, CT, 2009.
- (54) Becke, A. D. Density-functional thermochemistry. III. The role of exact exchange. *J. Chem. Phys.* **1993**, *98*, 5648–5652.
- (55) Lee, C. T.; Yang, W. T.; Parr, R. G. Development of the colle-salvetti correlation-energy formula into a functional of the electron density. *Phys. Rev. B* **1988**, *37*, 785–789.
- (56) Hay, P. J.; Wadt, W. R. Ab initio effective core potentials for molecular calculations. Potentials for K to Au including the outermost core orbitals. *J. Chem. Phys.* **1985**, *82*, 299–310.
- (57) Casida, M. E.; Jamorski, C.; Casida, K. C.; Salahub, D. R. Molecular excitation energies to high-lying bound states from time-dependent density-functional response theory: Characterization and correction of the time-dependent local density approximation ionization threshold. *J. Chem. Phys.* **1998**, *108*, 4439–4449.
- (58) Stratmann, R. E.; Scuseria, G. E.; Frisch, M. J. An efficient implementation of time-dependent density-functional theory for the calculation of excitation energies of large molecules. *J. Chem. Phys.* **1998**, *109*, 8218–8224.
- (59) Walters, V. A.; Hadad, C. M.; Thiel, Y.; Colson, S. D.; Wiberg, K. B.; Johnson, P. M.; Foresman, J. B. Assignment of the $\sim\text{A}$ state in bicyclobutane. The multiphoton ionization spectrum and calculations of transition energies. *J. Am. Chem. Soc.* **1991**, *113*, 4782–4791.
- (60) Caricato, M.; Mennucci, B.; Tomasi, J.; Ingrosso, F.; Cammi, R.; Corni, S.; Scalmani, G. Formation and relaxation of excited states in solution: A new time dependent polarizable continuum model based on time dependent density functional theory. *J. Chem. Phys.* **2006**, *124*, 124520–124533.
- (61) Mennucci, B.; Cappelli, C.; Guido, C. A.; Cammi, R.; Tomasi, J. Structures and Properties of Electronically Excited Chromophores in Solution from the polarizable continuum model coupled to the time-dependent density functional theory. *J. Phys. Chem. A* **2009**, *113*, 3009–3020.
- (62) Dennington, R. II.; Keith, T.; Millam, J. *Gauss View 3*; Semichem, Inc.: Shawnee Mission, KS, 2007.
- (63) O Boyle, N. M.; Tenderhol, A. L.; Langner, K. M. A library for package-independent computational chemistry algorithms. *J. Comput. Chem.* **2008**, *29*, 839–845.
- (64) Yujie, S.; Ojaimi, M. E.; Hammitt, R.; Thummel, R. P.; Turro, C. Effect of ligands with extended π -system on the photophysical properties of Ru(II) complexes. *J. Phys. Chem. B* **2010**, *114*, 14664–14670.
- (65) Sun, Y.; Turro, C. Highly Solvent Dependent Luminescence from $\text{Ru}(\text{bpy})_n(\text{dppp}2)_{3-n}]^{2+}$ ($n = 0–2$). *Inorg. Chem.* **2010**, *49*, 5025–5032.
- (66) Wachtler, M.; Kupfer, S.; Guthmuller, J.; Rau, S.; Gonzalez, L.; Dietzek, B. Structural control of photoinduced dynamics in 4 H-imidazole-ruthenium dyes. *J. Phys. Chem. C* **2012**, *116*, 25664–25676.
- (67) Schulze, B.; Escudero, D.; Friebel, C.; Siebert, R.; Görsl, H.; Sinn, S.; Thomas, M.; Mai, S.; Popp, J.; Dietzek, B.; González, L.; Schubert, U. S. Ruthenium(II) photosensitizers of tridentate click-derived cyclo-metalating ligands: a joint experimental and computational study. *Chem.—Eur. J.* **2012**, *18*, 4010–4025.
- (68) Siebert, R.; Andreas, W.; Schubert, U. S.; Dietzek, B.; Popp, J. The molecular mechanism of dual emission in terpyridine transition metal complexes-ultrafast investigations of photoinduced dynamics. *Phys. Chem. Chem. Phys.* **2011**, *13*, 1606–1617.